Dysregulation of macrophage PEPD in obesity determines adipose tissue fibro-inflammation and insulin resistance

Vanessa Pellegrinelli (✉ vp332@medschl.cam.ac.uk)
Institute of Metabolic Science

Segio Rodriguez-Cuenca
MRC Metabolic Diseases Unit, University of Cambridge

Christine Rouault
Sorbonne Université, INSERM, Nutrition and obesities; systemic approaches (NutriOmics)

Hanna Schilbert
Genetics and Genomics of Plants, Center for Biotechnology (CeBiTec) & Faculty of Biology, Bielefeld University

Sam Virtue
University of Cambridge

Jose Maria Moreno-Navarrete
Institut d'Investigació Biomèdica de Girona

Guillaume Bidault
University of Cambridge https://orcid.org/0000-0002-8396-9962

Maria del Carmen Vázquez Borrego
Maimonides Institute of Biomedical Research of Cordoba (IMIBIC)

Ana Rita Dias
Metabolic Research Laboratories, Institute of Metabolic Science, Addenbrooke's Hospital, University of Cambridge

Boas Pucker
Genetics and Genomics of Plants, Center for Biotechnology (CeBiTec) & Faculty of Biology, Bielefeld University

Martin Dale
University of Cambridge Metabolic Research Laboratories

Mark Campbell
University of Cambridge

Stefania Carobbio
Metabolic Research Laboratories, Institute of Metabolic Science, Addenbrooke's Hospital, University of Cambridge

Judith Aron-Wisnewsky

Assistance-Publique Hôpitaux de Paris, Nutrition department, Pitié-Salpêtrière hospital

Silvia Mora

Department of Molecular and Cellular Physiology, Institute of Translational Medicine, The University of Liverpool

Mauro Masiero

The Beijer Laboratory and Department of Immunology, Genetics and Pathology; Uppsala University and SciLifeLab

Anastasia Emmanouilidou

The Beijer Laboratory and Department of Immunology, Genetics and Pathology; Uppsala University and SciLifeLab

Subhankar Mukhopadhyay

MRC Centre for Transplantation Peter Gorer Department of Immunobiology School of Immunology & Microbial Sciences King's College

Gordon Dougan

University of Cambridge

Marcel den Hoed

he Beijer Laboratory and Department of Immunology, Genetics and Pathology; Uppsala University and SciLifeLab https://orcid.org/0000-0001-8081-428X

Ruth Loos

Mount Sinai School of Medicine https://orcid.org/0000-0002-8532-5087

José Manuel Fernández-Real

Department of Diabetes, Endocrinology and Nutrition, Girona Biomedical Research Institute (IDIBGI), University Hospital of Girona Dr Josep Trueta

Davide Chiarugi

Metabolic Research Laboratories, Institute of Metabolic Science, Addenbrooke's Hospital, University of Cambridge

Karine Clément

APHP https://orcid.org/0000-0002-2489-3355

Antonio Vidal-Puig (✉ **ajv22@medschl.cam.ac.uk**)

University of Cambridge https://orcid.org/0000-0003-4220-9577

Article

Keywords: Fibrosis, inflammation, macrophages, Prolidase, PEPD, Xaa-Pro dipeptidase, Obesity, adipose tissue, extracellular matrix, EGFR, exploratory factor analysis

Posted Date: August 24th, 2020

DOI: https://doi.org/10.21203/rs.3.rs-57182/v1

Abstract

Fibrosis is a hallmark of adipose tissue (AT) dysfunction and obesity-associated insulin resistance that results from an impaired collagen turnover. Peptidase D (PEPD) plays a vital role in collagen turnover by degrading proline-containing dipeptides. Nevertheless, its specific function and importance in AT is unknown. GWAS identified the rs731839 variant in the locus near PEPD that uncouples obesity from insulin resistance and dyslipidaemia, thus indicating that defective PEPD might impair AT remodelling and exacerbate metabolic complications. Here we show that in human and murine obesity, PEPD expression and activity decrease in AT, coupled to the release of PEPD systemically. Both events, in turn, are associated with the accumulation of fibrosis in AT and insulin resistance. Using pharmacologic and genetic animal models of PEPD down-regulation, we show that whereas dysfunctional PEPD activity provokes AT fibrosis, it is the PEPD secreted by AT the main contributor to inflammation, insulin resistance and metabolic dysfunction. Also, PEPD originated in inflammatory macrophages (M), plays an essential role promoting fibro-inflammatory responses via activation of EGFR in M and preadipocytes. Using genetic ablation of pepd in M that prevents obesity-induced PEPD release, also averts AT fibro-inflammation and obesity-associated metabolic dysfunctions. Taking advantage of factor analysis, we have identified the coupling of prolidase decreased activity and increased systemic levels of PEPD as the essential pathogenic triggers of AT fibrosis and insulin resistance. Thus, PEPD produced by M qualifies as a biomarker of AT fibro-inflammation and a therapeutic target for AT fibrosis and obesity-associated insulin resistance and type 2 diabetes.

Main

We measured *PEPD* mRNA expression in adipose tissue (AT) from seven human cohorts spanning a broad spectrum of BMIs, ages and degrees of insulin resistance (Extended data Figure 1a). *PEPD* expression was lower in visceral white AT (VsW) of obese individuals than in lean ones and also lower in obese type 2 diabetics than in obese normoglycemic patients (Figure 1a, b). *PEPD* was lower in VsW depot than in subcutaneous white AT (ScW) in a paired sample cohort study (Figure 1c) and lower *PEPD* expression in VsW was associated with higher BMI and collagen content in AT from obese individuals (measured as hydroxyproline levels, HPro) (Figure 1d). Moreover, low *PEPD* expression in VsW was also associated with lower expression of genes associated with AT insulin sensitivity such as *PLIN1*, *PPARG* and *GLUT4* (Extended data Table 1). These results suggested that PEPD may regulate AT collagen remodelling and metabolism in AT. The reduction of VsW *PEPD* expression in obese individuals was tightly coupled with higher PEPD serum levels than lean individuals and associated with higher total cholesterol and aspartate transaminase (ASAT) levels (Cohort 2e, Figure 1e; Extended data Figure 1b). Among obese subjects, those with the higher amount of PEPD released from VsW were more proned to insulin resistance and type 2 diabetes (Figure 1f; Extended data Figure 1c). Also, the ROC curve analysis highlighted the PEPD released from VsW (but not ScW) as a predictor to type 2 diabetes with a cut off for PEPD levels of 1.33µM (cohort 2e,f; Figure 1g). Re-analysis of serum proteomic data from insulin resistant and sensitive obese subjects[6] further confirmed the predictive value of PEPD for insulin

resistance and that serum PEPD levels were positively correlated with lipid metabolism (e.g. APOA proteins), inflammation and ECM remodelling proteins (e.g. DPP4, TNC, COL4A2) (Figure 1h, i; Extended data Figure 1d). Altogether, these data from human cohorts provided strong evidence for potential relevance of PEPD as a marker of fibro-inflammation and insulin resistance in obese individuals.

Similar pattern of low AT PEPD activity coupled with high circulating levels of PEPD was recapitulated in diet-induced obese mice with AT fibrosis and metabolic disturbances (e.g. high glycaemia, liver steatosis) (Extended data Figure 1e-i). Accordingly, serum levels of PEPD predicted the degree of fibrosis (peri-Ad collagen) and inflammation (*tnfa* expression) in GnW, with cut-off values for PEPD of 1.32 µM (Extended data Figure 1j).

To uncouple the effects of PEPD from obesity, we treated chow-fed lean mice with CBZ-Proline (CBZ-Pro), a selective pharmacological inhibitor of PEPD activity[7]. CBZ-Pro-treated mice showed higher dipeptides Gly-Pro serum levels confirming inhibition of PEPD activity and also exhibited higher PEPD serum levels than control mice (Figure 1j, k). CBZ-Pro-treated mice had similar body weight or fat mass (Extended data Figure 2b, c) but had more severe AT fibro-inflammation in GnW, and were more hyperglycaemic, glucose intolerant and insulin resistant compared to controls (Figure 1l-o; Extended data Figure 2d). Of note, on fasting, CBZ-Pro-treated mice showed fasting insulin and FFA blood levels comparable to controls (Extended data Figure 2e, f). The amount of PEPD into the serum of CBZ-Pro treated mice was positively correlated with the degree of ScW fibrosis and glycaemia in the fed state (Extended data Figure 2g). Altogether, these results show that both, downregulation of the intracellular PEPD activity in AT and concomitant increase in the serum levels of PEPD, were necessary and sufficient to induce AT fibro-inflammation and insulin resistance. Furthermore, in line with the human GWAS data, dysregulation of PEPD uncoupled fibro-inflammation and metabolic dysfunctions from obesity[3–5].

Given this dual role of PEPD, it remained unclear which event – i.e. decreased PEPD activity or increased PEPD released from the cells- was primarily responsible for AT fibrosis and/or metabolic alterations. We initially performed an Exploratory Factor Analysis (EFA). This is an unbiased statistical method, which establishes the cluster of biological variables with high loadings (correlation equivalent) on each specific factor in a reduced number of underlying variables ("factors") considered as "superfamilies of variables"[8]. Using EFA, we investigated how serum PEPD level/PEPD activity co-varied with the metabolic parameters measured in the CBZ-Pro-treated mice and controls (Figure 1p). EFA showed that factor 1, representing a cluster of AT fibrosis-related variables, co-varied with PEPD serum levels and fasting glucose levels. Moreover, factor 2, the cluster of "obesity"-related variables (BW, steatosis) also co-varied with PEPD serum levels, whereas factor 3 showed that the activity of GnW PEPD also co-varied with fasting glucose levels. Therefore, EFA indicated that the serum level of PEPD might explain the "fibrotic" profile and glycaemic status observed in CBZ-Pro mice.

The link between serum PEPD, fibrosis and glycaemia was further strengthened when we included the CBZ-Pro mice fed HFD 58% data in the EFA (Factor 1, Extended data Figure 2h). However, the co-variation between PEPD serum level and "obesity"-related variables was not sustained (Extended data Figure 2h).

We rationalised that since HFD *per se,* dysregulates PEPD activity/secretion, it was likely that HFD-fed control mice might have developed as strong fibro-inflammation as in CBZ-Pro-treated mice, masking the effects of this PEPD pharmacological inhibitor. Confirming this interpretation, untreated control and CBZ-Pro-treated mice fed HFD 58% exhibited similar severe AT collagen deposition, fasting insulin, FFA blood levels, glucose and insulin intolerance (Extended data Figure 2i-k).

Thus, to dissect the role of inhibition of PEPD activity from the extracellular action of the released PEPD, we next phenotyped the global *pepd* heterozygote (HET, +/-) and knock-out (KO, -/-) mice against their wild type (WT, +/+) littermates. PEPD activity and serum levels were not detected in *pepd* KO. Of interest, Pepd HET mice showed 50% decreased PEPD activity but no difference in PEPD serum levels compared to WTs (Figure 2a, b; Extended data Figure 3a, b) and were morphologically similar to WT. In contrast, *pepd* KO exhibited a runty phenotype characterised by short length, low body weight and decreased fat mass (Extended data Figure 3c-e) which complicated subsequent phenotyping. Thus, we preferentially used the *pepd* HET for metabolic analysis. We observed higher collagen accumulation in the ScW (HET/KO) and GnW (KO) compared to WT littermates in chow diet, supporting the role of reduced PEPD activity in promoting fibrosis (Figure 2c). This association was supported by correlation matrix analysis (Extended data Figure 3f). Moreover, EFA analysis of *pepd* KO mice fed chow diet showed that Factor 1, clustering GnW or ScW fibrosis-related variables, had strong loading of glucose blood levels and negative loading of PEPD activity in AT depots (Figure 2d).

The development of metabolic complications in the *pepd* HET mice (i.e. insulin resistance, increased FFA levels and liver steatosis) required challenging with HFD. Again, when on HFD no differences in BW and collagen deposition were observed among the genotypes (extended data Figure 3g-j and 4a). Feeding the *pepd* HET mice with HFD 45%, resulted in higher fed glucose levels and insulin intolerance compared to WT mice, despite maintaining similar fasted glucose, insulin and FFA levels (Extended data Figure 4b-d). When challenged with HFD 58%[9] promoting greater fibro-inflammation in GnW than HFD 45% (Extended data Figure 4e, f), *pepd* HET mice were more insulin resistant and exhibited a trend to be more glucose intolerant despite still showing significantly lower fasting glucose than WT mice (Figure 2e-g). On HFD 58%, *pepd* HET mice showed significantly higher FFA levels compared to WT mice, had AT insulin resistance according to the AT-insulin resistance index (AT-IR index)[10] (Figure 2g, Extended data Figure 4g), and exhibited more severe liver steatosis than WT (Extended data Figure 4h). Collectively, these results indicate that reduced PEPD activity in *pepd* HET mice was enough to develop AT fibrosis, in the absence of obesity, and that upon challenge with HFD -which downregulates PEPD activity, increases its release and promotes fibrosis - further exacerbated metabolic complications in HET mice. Moreover, EFA revealed that in *pepd* HET mice fed chow+HFD (45% and 58%), their insulin resistance and liver steatosis could be determined by BW and GnW fibrosis, since these variables clustered and co-varied together (Factor 2, Extended data Figure 5a, b).

To unmask the molecular mechanisms underlying the fibrogenic and metabolic pathogenic effectors driven by the downregulation of *pepd*, we performed RNA-Sequencing of the GnW of *pepd* HET and KO mice fed chow and HFD 45 %. We selected the milder nutritional challenge to prevent the confounding

fibro-inflammatory effect of 58% HFD by down-regulating *pepd* in WT mice (Extended data Figure 5c). Analysis of DEGs and the top pathways differentially regulated in GnW *pepd* HET and KO mice fed 45 %HFD *vs.* WT revealed that both *pepd* HET and KO mice had higher expression of genes involved in the regulation of actin cytoskeleton and cell cycle, immune system, inflammatory-related pathways, and ECM/ECM organisation-related proteins (Figure 2h, Extended data Figure 5d; Supplementary Information, Supplementary Table S2-S5). Also, *pepd* HET mice fed HFD 45% showed lower expression of genes involved in metabolic pathways including fatty acids, leptin and insulin signalling. The *pepd* KO mice also showed higher expression of genes in the cluster of pro-diabetes-related pathway. Validation of these data using additional *in vitro* and *ex-vivo* experiments confirmed that defects in PEPD activity impaired adipogenesis from GnW progenitors, lipolysis in mature adipocytes and leptin secretion from GnW tissue explants (Extended data Figure 5e-i).

Next, we focused on the analysis of DEGs related to AT function and fibro-inflammation regulated by HFD 45% on each genotype (WT, HET and KO) (Figure 2i; Extended data Figure 5j; Supplementary Information, Supplementary Table S6-S8). In response to HFD 45% and compared with chow diet, GnW of the *pepd* HET mice exhibited higher expression of pro-fibrotic, ECM components, ECM remodelling genes, and inflammatory and immune cells genes, whereas it had lower expression of AT metabolism-related genes. Transcriptomic analyses confirmed the exacerbated fibro-inflammation and AT dysfunction in both the KO and HET mice when challenged with HFD 45%. This fibro-inflammatory response to HFD was more exacerbated in HET mice than in WT, indicating that *pepd* HET mice were prone to fibro-inflammation in response to HFD. These results also indicated that M□ and immune cell-derived factors might contribute actively to the metabolic phenotypes associated with the genetic ablation of *pepd*, pointing to a pathogenic link between PEPD dysregulation and immunity regulation.

Cellular fractionation of GnW from lean mice revealed that M□ (CD11b+ fraction) reported the highest levels of *pepd* expression compared to that of mature adipocytes (AD), other immune (CD45+), endothelial cells (CD31+) or stroma-vascular fractions (SVF) (Figure 3a). In agreement with the results from total AT, the expression of *pepd* was lower in AT M□ from 16 weeks-old ob/ob mice and also from mice fed 20 weeks with HFD 45% compared with their controls (genetically lean and chow fed mice, respectively) (Extended data Figure 6a, b). Moreover, PEPD activity increased during M□ differentiation using a model of bone-marrow-derived M□ (BMDMs) (Extended data Figure 6c).

These findings were validated in humans by showing PEPD enrichment in the immune cell fraction ($CD45^+$) of human AT (Extended data Figure 6d). Also, proteomic analysis of human induced pluripotent stem cell-derived M□ (iPSDM), confirmed the relatively high abundance of PEPD in M□ compared to undifferentiated iPSCs (Extended data Figure 6e). Given that obesity is associated with an imbalance between classically activated M□ (considered as inflammatory) and alternatively activated M□ (considered as non-inflammatory), we assessed the modulation of *pepd* expression by specific M□ polarising agents[11]. In agreement with the reduction of *pepd* expression in the inflamed AT of obese mice, *pepd* expression was also lower in pro-inflammatory M(LPS) cells, whereas it was higher in M(GC), and not modulated in M(IL-4) treated cells compared to unstimulated M□ (Extended data Figure 6f). Additional

supportive evidence of human transferability was provided by RNA-Seq comparing undifferentiated human induced pluripotent stem cells (iPSCs) and differentiated [12] and analysis of the effect of LPS on human macrophage-derived monocytes (MDM) and iPSDM. In agreement with murine models, stem cell transcriptomic analysis confirmed that i) *PEPD* expression increases during human MΦ differentiation; ii) iPSDM and MDM display similar *PEPD* expression levels, and that iii) PEPD expression decreases in response to LPS treatment in both iPSDM and MDM(Extended data Figure 6g).

We then validated at the cellular level that BMDMs treated with CBZ-Pro or LPS, both known to decrease PEPD activity (Extended data Figure 6h), resulted in higher levels of PEPD released to the medium compared to non-activated or alternatively activated Mφ (Figure 3b; Extended data Figure 6i). These results strengthen the functional coupling between the lower enzymatic activity of PEPD in AT and higher release of PEPD to the extracellular compartment.

Based on these previous results, we investigated whether the released PEPD was a determinant of MΦ polarisation. Treatment of MΦ with purified PEPD protein-induced phosphorylation of NF-κB (ser536) and expression of inflammatory markers, such as *cox2* and *il-1β*, while non-inflammatory markers *mgl1* and *mrc2* were downregulated (Figure 3c; Extended data Figure 7a-d). Phospho-kinase proteome analysis using a profiler array on PEPD-treated BMDMs confirmed that PEPD phosphorylated EGFR (Extended data Figure 7e)[13]. Pre-treatment of MΦ with Erlotinib, an EGFR-specific tyrosine kinase inhibitor, attenuated PEPD-induced NFkB phosphorylation, as well as *cox2* and *il1β* expression (Figure 3d; Extended data Figure 7f, g). We rationalised that besides its effects on MΦ, secreted PEPD could also signal to other adipose tissue cells. We characterised the effect of extracellular PEPD on differentiated and non-differentiated pre-adipocytes, as critical pro-fibrotic cellular effectors in the AT[14,15]. Supporting a direct PEPD pro-inflammatory role, purified PEPD increased *il-6* expression in differentiated pre-adipocytes, promoted the production of collagen I and prevented lipid accumulation in pre-adipocytes in part through a mechanism involving EGFR signalling (Figure 3e, Extended data Figure 7h-j).

To dissect the pivotal role of PEPD secreted from MΦ driving fibro-inflammation and metabolic disturbances, we performed a bone marrow transplant (BMT) from *pepd* KO into WT recipient mice to ablate *pepd* exclusively in hematopoietic cells (HCs) (Figure 3f; Extended data Figure 8a). BMT KO mice showed 85% reduced prolidase activity in peritoneal MΦ and 50% reduction of prolidase activity in the whole AT (Figure 3g, h). Reduction in PEPD activity by genetic manipulation was not associated with increased PEPD levels in serum, opposite to what we observed in CBZ-Pro-treated mice or dietary models of obesity (Extended data Figure 8b).

As previously observed in models with decreased PEPD activity, the BMT KO model also had increased collagen accumulation in AT compared to BMT WT (Figure 3i). However, BMT KO mouse maintained carbohydrate metabolic homeostasis in contrast to the chow-fed CBZ-Pro-treated mice, in which the decreased PEPD activity was inversely associated to its secretion (Extended data Figure 8c-h). Furthermore, when fed 58% HFD, the BMT KO mice exhibited more significant fibrosis than BMT WTs but were resistant to obesity and associated fibro-inflammation and metabolic disturbances (i.e. glucose and

insulin tolerance, and liver steatosis) (Extended data Figure 8e-l). Thus, the BMT KO model exhibited increased AT fibrosis uncoupled from insulin resistance and liver steatosis. These results showed that fibrosis and metabolic complications could be uncoupled and pointed to the relevance of the extracellular PEPD produced by M as a critical trigger of fibro-inflammation and metabolic complications. Moreover, EFA among BMT mice fed chow, further confirmed the negative association between AT fibrosis and PEPD activity (Factor 1, Figure 3m). Also, factor 3 showed that AT insulin resistance-related parameters (i.e. AT-IR and FFA levels) co-varied with PEPD serum levels (Figure 3m). Thus, these results supported that extracellular PEPD was the main trigger for AT related metabolic dysfunctions.

Finally, we performed a global integrative EFA including the three PEPD *in vivo* experimental models (pharmacological, genetic and macrophage-specific genetic ablation) to dissect the main pathogenic factors linking specific PEPD dysregulation and metabolic and fibro-inflammatory differences. EFA, including chow-fed and chow+HFD fed animals, showed that Factor 1, clustering AT fibrosis-related variables had negative loading of AT PEPD activity and body weight (Figure 4a, c). Also, Factor 1 drove most of the differences between BMT and CBZ/PEPD mice (Figure 4b; Extended data Figure 9a). Factor 4, clustering insulin resistance-related variables had also negative loading with AT PEPD activity and explained differences between *pepd* mice and CBZ-Pro/BMT mice models (Figure 4a-d; Extended data Figure 9a, b). Finally, Factor 3, clustering AT insulin resistance had high loading of PEPD serum levels and explained the differences between CBZ-Pro and BMT/PEPD mice (Figure 4a-d).

These findings demonstrate for the first time that dysregulation of PEPD in obesity determines AT fibro-inflammation and exacerbates obesity-associated metabolic comorbidities through two independent but coupled mechanisms: i) PEPD enzymatic activity, promoting the last step in the degradation of collagen, is inhibited in M from obese AT leading to fibrosis and metabolic disturbances, i.e. liver steatosis and insulin resistance; and ii) secreted PEPD from M, acting as a non-canonical EGFR ligand promoting AT insulin resistance and fibro-inflammation in an autocrine and paracrine manner.

This study emphasises the pathogenic importance of defects in collagen degradation in obesity-associated complications. It provides a strong rationale for the measurement of serum PEPD in obese individuals to identify and stratify those at a higher metabolic risk -by recognising their susceptibility to adipose tissue fibrosis and inflammation. Taking advantage of *murine in vivo* models modelling dysregulated PEPD activity and secretion combined with EFA integrative analysis, our results strengthen the conclusion that dysregulation of PEPD elicits a dual role mediating AT fibrosis and metabolic risk through complementary mechanisms that open new avenues for both diagnostic and therapeutic approaches aiming at uncoupling obesity from its associated metabolic complications.

Methods

Human Studies

Age, BMI and glycaemic status of the different cohorts can be found in Figure S1a.

Cohort 1 and 3

In cohort 1, a group of 154 [84 visceral (VsW) and 70 subcutaneous (ScW) adipose tissues] from participants with a wide range of adiposity (BMI between 20 and 68 kg/m2), were analysed. In cohort 3, 46 VAT and 36 SAT samples from morbidly obese subjects (BMI > 35 kg/m2), were analysed. Altogether these subjects were recruited at the Endocrinology Service of the Hospital of Girona “Dr Josep Trueta”. All subjects were of Caucasian origin and reported that their body weight had been stable for at least three months before the study. Subjects were studied in the post-absorptive state. They had no systemic disease other than obesity and all were free of any infections in the previous month before the study. Liver diseases (specifically tumoral disease and HCV infection) and thyroid dysfunction were specifically excluded by biochemical work-up. All subjects gave written informed consent, validated and approved by the ethical committee of the Hospital of Girona “Dr Josep Trueta”, after the purpose of the study was explained to them. Samples included in this study were partially provided by the FATBANK platform promoted by the CIBEROBN and coordinated by the IDIBGI Biobank (Biobanc IDIBGI, B.0000872), integrated in the Spanish National Biobanks Network and they were processed following standard operating procedures with the appropriate approval of the Ethics, External Scientific and FATBANK Internal Scientific Committees. AT samples were obtained from SAT and VAT depots during elective surgical procedures (cholecystectomy, surgery of abdominal hernia and gastric by-pass surgery). Samples of AT were immediately transported to the laboratory (5-10 min). The handling of tissue was carried out under strictly aseptic conditions. AT samples were washed in PBS, cut off with forceps and scalpel into small pieces (100 mg), and immediately flash-frozen in liquid nitrogen before stored at -80ºC. Serum glucose concentrations were measured in duplicate by the glucose oxidase method using a Beckman glucose analyser II (Beckman Instruments, Brea, CA, United States). Intra-assay and inter-assay coefficients of variation were less than 4% for all these tests. Total serum triglycerides were measured by an enzymatic, colorimetric method with glycerol phosphate oxidase and peroxidase (Cobas TRIGL) using a Roche Hitachi Cobas c 711 instrument.

Cohort 2

ScW and VsW (omental) biopsy samples were obtained from severely obese (BMI >35 kg/m2) and lean subjects (BMI ≤25 kg/m2) who were undergoing elective surgery. Obese patients were candidate for bariatric surgery and the studies were conducted in Paris France and Spain in accordance with the Helsinki Declaration and approved by the Ethics Committee of Clinical Research (CPP Ile-de-France 1, Fibrota study N° clinical trial NCT01655017) and University Hospital of Girona Dr. Josep Tructa). All patients were characterized for detailed corpulence and metabolic phenotyping as described in[16]. Blood sampling were performed one month before the surgery at the fasting state. Paired AT samples (visceral and subcutaneous fat) were obtained at the time of the surgery by the same surgeon. Signed informed consents were obtained in all lean and obese individuals in agreement with ethic regulation.

Animals

Male C57Bl6/J mice were purchased from Charles River. *Pepd* KO mice were generated by the Wellcome Trust Sanger Institute Mouse Genetics Project on a C57Bl6/J background by mating heterozygous mice. Wild type and leptin deficient mice, $Lep^{Ob/Ob}$, were on a C57BL/6 background. Studies were conducted in 8-28 weeks old mice using littermate controls. This research has been regulated under the Animals (Scientific Procedures) Act 1986 Amendment Regulations 2012 following ethical review by the University of Cambridge Animal Welfare and Ethical Review Body (AWERB). Mice were housed 3–4 per cage in a temperature-controlled room (21°C) with a 12 hr light/dark cycle, with 'lights on' corresponding to six am. Animals had ad-libitum access to food and water. A standard chow diet (DS-105, Safe Diets) was administered to all animals from weaning, consisting of 64.3% carbohydrate, 22.4% protein and 13.3% lipid of total calories. Only male mice were used for in vivo experiments and preparation of BMDMs.

Generation of Bone Marrow Chimeras

C57BLl6/J mice at 10 weeks of age received a sub-lethal dose of whole-body irradiation (9 Gy). The day after irradiation, donor *pepd* KO mice were culled, and their femurs and tibias were removed aseptically. Marrow cavities were flushed in RPMI medium, and single-cell suspensions were prepared. The irradiated recipients received 1×10^7 bone marrow cells in 0.1 ml of PBS by tail vein injection. During 4 weeks after BMT, Bactrim (Roche) was added to drinking water. After 2 additional weeks, mice were switched to HFD 58%. Mice were culled 16 weeks later to collect blood and tissues.

Diets and Pharmacological challenges

Diets for animal studies included standard chow (10% calories from lipid), HFD 45% (D12451, Research Diets, 45% calories from lipid) and HFD 58% (D12331, Research Diets, 58% calories from lipid). Standard chow or HFD was provided ad libitum to animals from 8weeks old until indicated. Regarding PEPD pharmacological inhibition in vivo, 8 weeks-old C57BLl6/J mice were first fed with chow for 10 weeks. CBZ-Pro supplemented pellets were prepared fresh every other day in house by spraying homogeneously a solution of CBZ-Proline (2mM) in 70% ethanol solution. Mice consumed (when pellets were dry) an approximatively daily dose of 60mg/kg of CBZ-Proline, as previously used in other murine studies[7] , treatment lasted for 6 weeks, control mice were offered regular pellets. CBZ-Proline does not alter viability or promote toxic effects in mice [7]. In our experimental conditions, CBZ-Pro-treated mice did not show evidence of hepatotoxicity/liver damage (alanine (ALAT) or aspartate (ASAT) transaminase levels) (Extended data Figure 2a).

Body Composition

Fat and lean masses were calculated by time-domain nuclear magnetic resonance (TD-NMR) by using a minispec Live Mice Analyzer LF50 (Bruker).

Glucose and Insulin Tolerance Tests

For glucose tolerance test, mice were fasted for overnight with free access to drinking water. Glucose was administered intraperitoneally (2 g/kg), and blood glucose levels were monitored from the tip of the tail with a glucometer. For insulin tolerance tests, insulin was administered intraperitoneally (0.75mU/g), and blood glucose was measured at various times after injection.

Serum Biochemistry

Triglycerides were measured on the Dimension RXL analyzer (Siemens Healthcare). Free fatty acids were measured using the Roche Free Fatty Acid Kit (half-micro test) (kit code 11383175001). Insulin was measured using electrochemical luminescence immunoassay on the MesoScale Discovery immunoassay platform.

Explants for conditioned medium

Approximately 100 mg of freshly dissected GnW cut into fine pieces from 30-week-old mice in chow and HFD conditions were incubated for 6h hour at 37oC in 5% CO2 in DMEM with 5% heat inactivated FBS, 20 mM HEPES, 100 units/mL penicillin, 100 µg/mL streptomycin, and 20 mM L-glutamine) (1 mL media per 100 mg of tissue).

Magnetic-activated cell sorting

ScW, GnW and BAT from 10-12 weeks old C57BL/6 mice were dissociated by collagenase treatment isolating unilocular adipocytes from the stromavascular fraction (SVF). SVF was resuspended in MACS buffer (PBS, 2mM EDTA (sterile), 0.5% Bovine Serum Albumin) and incubated with Microbeads conjugated to monoclonal antihuman/mouse CD11b (Mac-1α) antibodies (isotype: rat IgG2b, Miltenyi Biotech). $Cd11^{+}$ fractions were isolated using MACS LS columns according to manufacturer instructions (Miltenyi Biotech).

Bone marrow derived M preparation and treatments

Femur and tibia bones from 10-16 weeks-old C57BL6 mice or *pepd* WT, HET and KO mice were isolated and cleaned, and 10 mL of RPMI-1640 was flushed through each bone using a syringe. Total bone-marrow cells were passed into a 100 µm cell strainer and counted using Countess II automated cell counter (Thermofisher). Cells were spun (400g, 5 min.), resuspended in BMDM culture medium (RPMI1640 supplemented with 20% of L929-conditioned cell medium, 10% heat-inactivated foetal bovine serum (HI-FBS), and 1% penicillin and streptomycin). Total bone-marrow cells were seeded in 10 cm non-culture treated plates (Falcon) at a density of $5x10^{6}$ cells per plate per 10 ml of Mφ differentiation medium and cultured for 7 days at 37 °C in 5% CO2. On day 5 of differentiation, medium was removed and replace with 10 ml of fresh BMDM culture medium. On day 7, BMDMs were detached using ice-cold PBS-EDTA 1mM, spun (400xg, 5 min.) and resuspended in fresh BMDM culture medium. Differentiated BMDMs were counted using Countess II automated cell counter and cell concentration adjusted to 5x105 cells/ml. Immediately after, cells were plated for experiments at the following densities: 100µl/well of 96-

well plate, 500 µl/well of 24-well plate, 1 ml/well of 12-well plate, 2 ml/well of 6-well plate and 10 ml per 10 cm plate. Cells were incubated for 16-24 h after plating before conducting experiments.

Mφ purity of the culture was routinely tested by the expression of CD11b and F4/80 by flow cytometry. 93-97% of the cells express high levels of CD11b and F4/80 after 7 days of differentiation.

To make L929-conditioned medium, L929 cells (CCL-1, ATCC) were seeded in DMEM supplemented with 10% heat-inactivated FBS, 100 U/ml penicillin-streptomycin and 2 mM L-glutamine (Sigma) at a density of 250,000 cells per 50 ml of medium per T175 tissue culture flask. Medium was harvested after 1 week of culture, and then 50 mL of fresh DMEM supplemented with 10% heat-inactivated FBS, 100 U/ml penicillin-streptomycin and 2 mM L-glutamine was added onto cells and harvested 1 week later. Batches obtained after the first and second weeks of culture were mixed at a 1:1 ratio, aliquoted and stored at -20 °C.

After differentiation, BMDMs were cultured in 12 well-culture plate (5 X 10^5 cell) for 24h in BMDM medium before 6-24h stimulation with LPS (100ng/mL), DEX (100nM), IL4 (10ng/mL), purified PEPD (250nM), Gly-Pro (10mM) or CBZ-Pro (6mM) and stored -80 C prior RNA extraction or prolidase assay. Erlotinib (5µM) was added to the culture medium 2h before and during the treatment with PEPD. We validated PEPD specific effect by measuring *cox2* expression in BMDMs, reported as a PEPD target gene[13]. In addition, we discarded the potential cytotoxic effects of purified PEPD on BMDMs and its potential endotoxin contamination by boiling the purified protein and tested on BMDMs for *cox2* induction (Extended data Figure 7a-c).

iPS and monocyte-derived M□ differentiation and proteomic analysis

Human blood for monocyte-derived M□ was obtained from NHS Blood and Transplant, UK as described[12] and all experiments were performed according to guidelines of the University of Oxford ethics review committee. Undifferentiated human iPS cell line was maintained on a monolayer of mitotically inactivated mouse embryonic feeder (MEF) cells in Advanced Dulbecco's modified Eagles/F12 medium (DMEM/F12), supplemented with 20% Knockout replacement serum (KSR), 2mM L-Glutamine, β-mercaptoethanol (0.055 mM) and 8 ng/ml recombinant human FGF2 (RnD system); and differentiated into MΦ as described previously[17]. Briefly, this protocol involves key stages of differentiation- i) formation of 3 germ layer containing embryoid bodies (EBs) from iPSCs on withdrawing FGF, ii) long term production of myeloid precursor cells from EBs in presence of 25ng/ml IL-3 and 50ng/ml M-CSF (both RnD) and iii) terminal differentiation and maturation of myeloid precursors into matured MΦ in the presence of higher concentrations of M-CSF (100ng/ml). Protein preparation and proteomic analysis (PXD001953) were performed as described previously[18,19]. Methods and dataset from the RNAseq (EGAS00001000563) have been described in detail previously[12].

Cell Culture and adipocyte differentiation

Primary adipocytes isolated from GnW of 10 weeks-old pepd WT,HET, KO and 3T3L1 Cells were differentiated into adipocytes (day 9) accordingly to the protocol described by Roberts *et al.*[20].

Prolidase activity

Prolidase activity was determined optimizing Myara's spectrophotometric procedure which was modified from the Chinard technique[21,22] and miniaturised in 96 acid resistant well plates. Briefly, Tissue and M cell extracts were mixed V/V with PBS 50 mM HEPES/1mM MnCl2 and 0.75 mM GSH and incubated 20 min at 50 C. The activated mixture was then added V/V to PBS 94 mM glycyl-proline (Gly-Pro) for a final concentration of 47 mM and incubated or not (control corresponding to basal levels of proline in the cell/tissue extracts) 60 min at 37°C. Reaction was stopped by adding 6V of 0.45 M trichloroacetic acid and centrifuged at 4300 rpm for 60 min. The supernatant (1V) was then added to 4V of a 1:1 mixture of glacial acetic acid and Chinard's reagent (25 g of ninhydrin dissolved at 70 °C in 600 ml of glacial acetic acid and 400 ml of 6 M orthophosphoric acid) and incubated 15-45 min at 90 C. Absorbance was read at 515nm and proline concentration was calculated using proline standards ranged from 0.5 µg to 32 µg. Enzyme activity was reported in micromole of proline released per minute per milligram of protein.

GC-MS analysis of amino acids

Plasma and GnW explants samples were analysed for free amino acid concentrations using the EZ:faast GC-MS Kit (KGO-7166 Phenomenex Inc., Torrance, CA, USA). See Supplementary Information, Supplementary Methods.

Histological Analysis

AT and liver samples were fixed in 4% paraformaldehyde for 24h, embedded in paraffin, sectioned into 5 µm sections, and processed for Sirius (fibrosis) or haematoxylin and eosin (H&E) (liver steatosis) staining. The slides were scanned (Microscopy Zeiss Axioscan Z1 Slidescanner) and processed for fibrosis (Sirius staining excluding vessels) and steatosis (Vacuole % area) quantification using HALO™ Image Analysis Software.

Hydroxyproline Assay

Hydroxyproline measurement was done using a hydroxyproline colorimetric assay (BioVision) as previously described[23]. Briefly, frozen fat is weighted and heated in 6 N HCl at 110°C overnight in sealed tubes, as 10 µL of HCl/mg of WAT. Ten microliters are evaporated before incubation with chloramine-T and p-di-methyl-amino-benzaldehyde (DMAB) at 60°C for 90 min. The absorbance was read at 560 nm and the concentration was determined using the standard curve created with hydroxyproline.

ELISA assays

Murine and human PEPD protein concentration were measured using respectively an ELISA kit for Mouse Xaa-Pro dipeptidase (PEPD) ELISA kit (CSB-EL017784MO, CUSABIO) and Human PEPD (Peptidase D)

ELISA Kit (E-EL-H5575.96, Elabscience) in AT explant (from which debris was removed by centrifugation) and serum according to the manufacturer's instructions. A standard curve was prepared according to the manufacturer's instructions, and the value associated with an unconditioned media blank was subtracted from that of conditioned media.

RNA Extraction and Real-Time PCR

RNA from cells extracted using RNeasy Mini columns (Qiagen) according to the manufacturer's instructions. RNA was harvested from frozen tissue using RNA-STAT-60TM (AMS Bio), and purified by chloroform extraction and isopropanol precipitation. Reverse transcription was performed using Reverse Transcriptase System (Promega) according to manufacturer's instructions. Real-time PCR was carried out using TaqMan or Sybr Green reagents using an Abi 7900 real-time PCR machine using default thermal cycler conditions. Primer sequences are described in Table S9. Reactions were run in duplicate checked for reproducibility, and then averaged. A standard curve generated from a pool of all cDNA samples was used for quantification. The expression of genes of interest was normalized using the geometric average of four housekeeping genes (18s, 36b4, βactin, and B2m), and data is expressed as arbitrary units.

Regarding human samples (Cohorts 1, 2, 3), RNA purification, gene expression procedures and analyses were performed, as previously described[24,25]. Briefly, Total RNA was extracted and purified using RNeasy Lipid Tissue Mini kit and integrity was checked by Agilent Bioanalyzer. Total RNA was quantified by means of a spectrophotometer. The same amount of total RNA was reverse transcribed to cDNA from all samples using High Capacity cDNA Archive kit following manufacturers' instructions. Gene expression was assessed by real-time PCR using a LightCycler 480 real-time PCR system, using TaqMan and SYBRgreen technology suitable for relative genetic expression quantification. The commercially available and pre-validated TaqMan primer/probe sets used are described in Supplementary Information, supplementary Table 9 and 10).

RNA sequencing

Library preparation and sequencing

Total RNA of GnW was extracted using the miRNeasy mini kit (Quiagen) according to manufacturer's instructions. Per experiment, 4-10 independent biological repeats were used.

Total RNA was quality checked (RIN >7) via the Agilent Bioanalyser 2100 system, using the Agilent RNA 6000 Nano Kit. 1ug of RNA was used to construct barcoded sequencing libraries with the TruSeq Stranded mRNA HT Sample Prep Kit (Illumina) following supplier's instruction. All the libraries were validated using the Agilent Bioanalyser DNA 12000 and then multiplexed and sequenced on two lanes of Illumina HiSeq 4000 at SE50 at CR-UK Cambridge Institute Genomics Core Facility.

Processing of RNA-Seq data

RNA-Seq reads (Supplementary Information, supplementary Table 1) were mapped to the most recent ENSEMBLE version GRCm38.p5 of the mouse reference genome sequence (GRCm38.p5) using STAR v2.5.1b[26] including the annotations as hints for exon-intron borders. Reads were considered as mapped, if the similarity was at least 95% over at least 90% of the read length as previously described[27]. FeatureCounts v1.5[28] was applied for the generation of count tables based on the mapping files. Customized python scripts[27] were deployed for downstream processing including the normalization of the raw counts to the total number of assigned reads per gene (TPMs) and to the combined exon length (FPKMs), respectively.

Gene expression and pathway enrichment analyses

Raw counts were subjected to differential gene expression analysis via DESeq2[29] and different R packages (Supplementary software). Genes, which showed raw counts lower of equal to 2 in 50 % of all samples, were removed prior to the differentially expressed analysis. Wald test was applied to extract differentially expressed genes (DEGs, Supplementary Information, supplementary Table 2, 3, 6-8). Obtained DEGs were annotated via customized python scripts. Pathway enrichment analyses were performed with PIANO[30], using the gene set collection C2 retrieved from the Molecular Signatures Database (MSigDB)[31,32] (Supplementary Information, supplementary Table 4, 5). Bonferroni and Holm method was applied to correct for multiple testing.

Western Blotting

Proteins were extracted from tissue in lysis buffer (20 mM Tris-HCl, 150 mM NaCl, 1 mM EDTA, 1 mM EDTA, 1% Triton X-100, pH 7.5) with added protease inhibitor (Roche) and phosphatase inhibitor (Roche) cocktails. Debris and fat were cleared from lysates by centrifugation. Protein concentration was determined by Dc Protein assay (Bio- Rad). After dilution in Laemmli buffer with 0.5% 2-mercaptoethanol, 30 µg protein was loaded per well and subjected to SDS-PAGE in a 4%–12% gradient gel using the Novex NuPage midi system (Life Technologies) and transferred using the iBlot transfer system and reagents (Life Technologies). Membranes were blocked for 1 hour in 3% BSA in tris-buffered saline at room temperature, and incubated overnight at 4^{o}C with the appropriate primary antibody (see Supplementary Information, supplementary Table 9). Bound primary antibodies were detected using peroxidase-coupled secondary antibodies and enhanced chemiluminescence (Millipore). Blots were exposed digitally using the ChemiDoc MP System (Bio-Rad), and bands were quantified using Image J software. The expression of proteins was normalized to protein levels of a housekeeping protein (β-actin or Tubulin), and data is expressed as arbitrary units.

Array based detection of phosphorylated receptor tyrosine kinase

The Proteome Profiler Mouse Phospho-RTK Array Kit (R&D Systems, USA, Catalog Number: ARY014) was employed to screen for the level of phosphorylation of receptor tyrosine kinase (RTKs) in BMDMs in response to purified PEPD, according to the manufacturer's instructions. Briefly, the array membranes

were incubated 1h with an array blocking buffer prior incubation over night at 4C on an orbital shaker with 1.5 ml of cellular extract. The membrane were then washed and incubated 30 min. with streptavidin-HRP solution. Membranes were exposed digitally using the ChemiDoc MP System (Bio-Rad), and spots were quantified using the Image J software. One condition corresponds to a pool of cellular extracts from 4 independent experiments. All the arrays were measured three times; each spots were normalized to the positives controls. The results are presented in a heat map and considered relevant when the fold variation was >1.3 or <0.6.

Cytotoxicity assays

To determine the cytotoxic effect of compounds on M□, cells were seeded in Roswell Park Memorial Institute (RPMI) 1640 Medium without FBS supplemented at a density of 15,000 cells per well in wells of a 96 well plate. Cells were treated with the given compounds at the given concentrations for 24 hours, and cytotoxicity was measured using an LDH-Cytotoxicity Calorimetric Assay Kit (BioVision) according to the manufacturer's instructions.

Data Analysis

All data from experiments is summarised by its mean, with error bars showing standard error of the mean. The number of replicates is reported in the figure legends. When the results of a pairwise comparison is expressed as a fold-change it is declared in the figure legends to what value the data was normalised. Statistical analysis was performed using Prism7 and Prism8 (GraphPad). Comparisons between two groups were conducted using an unpaired t-test. Comparison between more than two groups were conducted using a one-Way ANOVA followed by appropriate post hoc multiple comparisons tests. Comparisons between more than two groups and factors were conducted using a two-way ANOVA followed by appropriate post hoc testing. Multiple comparisons were corrected and the resulting p-values were adjusted (q-value) relying on the two-stage linear step-up procedure of Benjamini, Krieger and Yekutieli. Pearson's coefficients were evaluated to estimate the extent of correlation between series of data. Data points were excluded ifrom the correlation analysis f they exhibited a value of more than two SDs from the mean. For all metabolic tests, the model animals were randomly assigned to the different experimental settings (GTT, ITT). Areas under the receiver operating characteristic (ROC) curves were determined for each variable to identify the predictors of AT fibro-inflammation and insulin resistance/type 2 diabetes. ROC curves is a plot of sensitivity (true positive) versus 1−specificity (false positive) showing the ability of biomarker (PEPD level) to discriminate between true positives (e.g. insulin resistant) and true negatives (e.g. insulin sensitive). The best marker has an ROC curve shifted to the left with area under the curve close to unity[33]. To determine the optimal cut-off values for fibro-inflammatory status or insulin resistance indices, the Youden index was calculated (sensitivity + specificity−1), and the values for the maximum of the Youden index was considered as the optimal cut-off points using the Web-tool easyROC[34]. Statistical significance was set at *p <0.05, **p<0.01 and ***p<0.001.

Exploratory Factor Analysis

Exploratory factor analysis (EFA) was conducted to determine the possible latent structure of the variables (listed, e.g., in Figure 1.p – rows of the depicted matrix) measured in each animal models, i.e., *pepd* mice, CBZ-Pro-treated mice and BMT mice. Factor analysis identifies a minimum number of new variables (factors) which are linear combinations of the original (measured) ones such that the new (fewer) variables contain most or all of the information and can facilitate the interpretation of a complex multivariate scenario. First, a matrix of correlation coefficients is computed and, from it, a set of main components (factors) is extracted. The relationships between the original variables and the factors is expressed in terms of "factor loadings" which, broadly speaking, can be interpreted as an estimate of the degree of correlation between the original variables and the factors.

We determined whether our data were appropriate for EFA by using the Kaiser–Meyer–Olkin (KMO) measure of sampling adequacy and Bartlett's test of sphericity (REF). Data were considered appropriate if the KMO was >0.7 and Bartlett's test was significant at $P < 0.05$. To determine the number of factors to retain we decided to rule out the components associated with eigenvalues less than 1. Parallel analysis confirmed that our choice was viable. Factors extraction was computed using the Maximum Likelyhood Estimate (MLE) method, implemented in the function fa of the psych R package[35]. Plots were produced either using in house scripts or using built-in functions of the FactoMineR R package[36].

Principal components analysis

Principal components analysis of the Lukk and the own dataset were calculated in R version 3.1.2 using the *prcomp* function of the *stats* package[37].

Declarations

Acknowledgments. This work was funded by Wellcome-Trust strategic award [100574/Z/12/Z], MRC MDU (MC_UU_12012/2), H2020 EPoS (Elucidating Pathways of Steatohepatitis-Grant Agreement 634413- and the British Heart Foundation (RG/18/7/33636). The Disease Model Core, Biochemistry Assay Lab the Histology Core and the Genomics and Transcriptomics Core are funded by MRC_MC_UU_12012/5 and a Wellcome-Trust Strategic Award [208363/Z/17/Z]. We thank the Wellcome-Trust Sanger Institute Mouse Genetics Project (Sanger MGP) and its funders for providing the mutant mouse line (Pepd<tm1a(KOMP)Wtsi. Funding and associated primary phenotypic information may be found at www.sanger.ac.uk/mouseportal." We thank the Disease Model Core from the Wellcome-MRC Institute of Metabolic Science and Agnes Lukasik for their technical assistance in the animal work. All animal work was carried out in the Disease Model Core (MRC Metabolic Diseases Unit [MRC_MC_UU_12012/5]; Wellcome-Trust Strategic Award [100574/Z/12/Z]). We also thank Genomics and Transcriptomics core, the Histology core and Gregory Strachan from the Imaging core for their technical assistance. All serum biochemistry was conducted by the Biochemistry Assay Lab (MRC Metabolic Diseases Unit [MRC_MC_UU_12012/5]). Clinical studies in France were supported by Contrat de Recherche Clinic (CRC APHP, Fibrota to JAW and KC), by National Agency of Research (ANR-Captorto KC) and by EFSD (to KC). KC was funded by H2020 EPoS (Elucidating Pathways of Steatohepatitis-Grant Agreement 634413. MD

receives funding from the National Institute for Health Research [Cambridge Biomedical Research Centre at the Cambridge University Hospitals NHS Foundation Trust]. We also thank all the patients and their physicians, the Dr. Laurent Genser for the surgical procedures, Prof Christine Poitou for patient recruitment and Dr Florence Marcheli for data management. Ruth JF Loos is supported by a grant from the NIH (R01DK107786). MdH is a fellow of the Swedish Heart-Lung Foundation (20170872) and a Kjell and Märta Beijer Foundation researcher. He is supported by project grants from the Swedish Heart-Lung Foundation (20140543, 20170678, 20180706) and the Swedish Research Council (2015-03657, 2019-01417). We acknowledge Dr. Chris Lelliott for access to *Pepd* mice samples.

We want also to acknowledge the FATBANK platform promoted by the CIBEROBN and the IDIBGI Biobank (Biobanc IDIBGI, B.0000872), integrated in the Spanish National Biobanks Network, for their collaboration and coordination.

The funders had no role in study design, data collection and interpretation, or the decision to submit the work for publication.

Please note that the views expressed are those of the authors and not necessarily those of the NHS, the NIHR or the Department of Health and Social Care.

Author Contributions. VP developed the hypothesis, designed the experiments, performed the experimental work, collected and analysed the data, coordinated and directed the project, created the images, wrote manuscript. SRC designed and conducted part of experimental work and edited the manuscript. CR and J-MM-N performed and analyzed human experiments. SV performed the bone marrow transplant in mice and the GC-MS for the detection of imidopeptides. HS, GB, MCV-B, ARD, MD,MC, SC,SM[11], MMM, AE, SM[13], MdH conducted experiments. JA-W and KC supervised enrolment and clinical phenotyping of obese subjects. HS, BP, DC performed bioinformatics analysis. DC also edited the manuscript. GD, RL, JMF and KC provided access to human data and discussed the manuscript. AVP developed the hypothesis, coordinated and directed the project, wrote the manuscript and is the guarantor of this work and, as such, had full access to all the data in the study and takes responsibility for the integrity of the data and the accuracy of the data analysis. All authors critically reviewed and edited the manuscript. The authors declare no competing interests.

Additional Information

Data availability. Data that support the findings of this study, including the scripts used for the analysis of the RNA-seq can be found at https://github.com/bpucker/RNA-Seq_analysis. DEGs and pathways from RNA-seq analysis can be found in supplemental tables. All other relevant data are available from the corresponding author on reasonable request.

Supplementary Information: This manuscript contains Supplementary Tables 1-8 and Supplementary Methods. Supplementary Information is available in the online version of the paper.

Reprints and permissions information is available at www.nature.com/reprints.

References

1. Sun, K., Tordjman, J., Clément, K. & Scherer, P. E. Fibrosis and adipose tissue dysfunction. *Cell Metab.* **18**, 470–477 (2013).
2. Kitchener, R. L. & Grunden, A. M. Prolidase function in proline metabolism and its medical and biotechnological applications. *J. Appl. Microbiol.* **113**, 233–247 (2012).
3. Manning, A. K. *et al.* A genome-wide approach accounting for body mass index identifies genetic variants influencing fasting glycemic traits and insulin resistance. *Nat. Genet.* **44**, 659–669 (2012).
4. Willer, C. J. *et al.* Discovery and refinement of loci associated with lipid levels. *Nat. Genet.* **45**, 1274–1283 (2013).
5. Yaghootkar, H. *et al.* Genetic evidence for a normal-weight 'metabolically obese' phenotype linking insulin resistance, hypertension, coronary artery disease, and type 2 diabetes. *Diabetes* **63**, 4369–4377 (2014).
6. Choi, H. *et al.* Plasma Protein and MicroRNA Biomarkers of Insulin Resistance: A Network-Based Integrative -Omics Analysis. *Front Physiol* **10**, 379 (2019).
7. Lupi, A. *et al.* N-benzyloxycarbonyl-L-proline: an in vitro and in vivo inhibitor of prolidase. *Biochim. Biophys. Acta* **1744**, 157–163 (2005).
8. Yong, A. G. & Pearce, S. A Beginner's Guide to Factor Analysis: Focusing on Exploratory Factor Analysis. *TQMP* **9**, 79–94 (2013).
9. Small, L., Brandon, A. E., Turner, N. & Cooney, G. J. Modeling insulin resistance in rodents by alterations in diet: what have high-fat and high-calorie diets revealed? *Am. J. Physiol. Endocrinol. Metab.* **314**, E251–E265 (2018).
10. Søndergaard, E., Espinosa De Ycaza, A. E., Morgan-Bathke, M. & Jensen, M. D. How to Measure Adipose Tissue Insulin Sensitivity. *J. Clin. Endocrinol. Metab.* **102**, 1193–1199 (2017).
11. Murray, P. J. *et al.* Macrophage activation and polarization: nomenclature and experimental guidelines. *Immunity* **41**, 14–20 (2014).
12. Alasoo, K. *et al.* Transcriptional profiling of macrophages derived from monocytes and iPS cells identifies a conserved response to LPS and novel alternative transcription. *Sci Rep* **5**, 12524 (2015).
13. Yang, L. *et al.* Prolidase directly binds and activates epidermal growth factor receptor and stimulates downstream signaling. *J. Biol. Chem.* **288**, 2365–2375 (2013).
14. Keophiphath, M. *et al.* Macrophage-secreted factors promote a profibrotic phenotype in human preadipocytes. *Mol. Endocrinol.* **23**, 11–24 (2009).
15. Iwayama, T. *et al.* PDGFRα signaling drives adipose tissue fibrosis by targeting progenitor cell plasticity. *Genes Dev.* **29**, 1106–1119 (2015).
16. Bel Lassen, P. *et al.* The FAT Score, a Fibrosis Score of Adipose Tissue: Predicting Weight-Loss Outcome After Gastric Bypass. *The Journal of Clinical Endocrinology & Metabolism* **102**, 2443–2453

(2017).

17. van Wilgenburg, B., Browne, C., Vowles, J. & Cowley, S. A. Efficient, long term production of monocyte-derived macrophages from human pluripotent stem cells under partly-defined and fully-defined conditions. *PLoS ONE* **8**, e71098 (2013).
18. Blohmke, C. J. *et al.* Interferon-driven alterations of the host's amino acid metabolism in the pathogenesis of typhoid fever. *J. Exp. Med.* **213**, 1061–1077 (2016).
19. Thomas, D. C. *et al.* Eros is a novel transmembrane protein that controls the phagocyte respiratory burst and is essential for innate immunity. *J. Exp. Med.* **214**, 1111–1128 (2017).
20. Roberts, A. W. G-CSF: a key regulator of neutrophil production, but that's not all! *Growth Factors* **23**, 33–41 (2005).
21. Besio, R. *et al.* Improved prolidase activity assay allowed enzyme kinetic characterization and faster prolidase deficiency diagnosis. *Clin. Chim. Acta* **412**, 1814–1820 (2011).
22. Myara, I., Charpentier, C. & Lemonnier, A. Optimal conditions for prolidase assay by proline colorimetric determination: application to iminodipeptiduria. *Clin. Chim. Acta* **125**, 193–205 (1982).
23. Marcelin, G. *et al.* A PDGFRα-Mediated Switch toward CD9(high) Adipocyte Progenitors Controls Obesity-Induced Adipose Tissue Fibrosis. *Cell Metab.* **25**, 673–685 (2017).
24. Moreno-Navarrete, J. M. *et al.* Insulin Resistance Modulates Iron-Related Proteins in Adipose Tissue. *Dia Care* **37**, 1092–1100 (2014).
25. Reggio, S. *et al.* Increased Basement Membrane Components in Adipose Tissue During Obesity: Links With TGFβ and Metabolic Phenotypes. *The Journal of Clinical Endocrinology & Metabolism* **101**, 2578–2587 (2016).
26. Dobin, A. *et al.* STAR: ultrafast universal RNA-seq aligner. *Bioinformatics* **29**, 15–21 (2013).
27. Haak, M. *et al.* High Quality de Novo Transcriptome Assembly of Croton tiglium. *Front Mol Biosci* **5**, 62 (2018).
28. Liao, Y., Smyth, G. K. & Shi, W. The Subread aligner: fast, accurate and scalable read mapping by seed-and-vote. *Nucleic Acids Res.* **41**, e108 (2013).
29. Love, M. I., Huber, W. & Anders, S. Moderated estimation of fold change and dispersion for RNA-seq data with DESeq2. *Genome Biol.* **15**, 550 (2014).
30. Väremo, L., Nielsen, J. & Nookaew, I. Enriching the gene set analysis of genome-wide data by incorporating directionality of gene expression and combining statistical hypotheses and methods. *Nucleic Acids Res.* **41**, 4378–4391 (2013).
31. Liberzon, A. *et al.* Molecular signatures database (MSigDB) 3.0. *Bioinformatics* **27**, 1739–1740 (2011).
32. Subramanian, A. *et al.* Gene set enrichment analysis: a knowledge-based approach for interpreting genome-wide expression profiles. *Proc. Natl. Acad. Sci. U.S.A.* **102**, 15545–15550 (2005).
33. Grund, B. & Sabin, C. Analysis of biomarker data: logs, odds ratios, and receiver operating characteristic curves. *Curr Opin HIV AIDS* **5**, 473–479 (2010).

34. Dincer Goksuluk, Selcuk Korkmaz, Gokmen Zararsiz & A. Ergun Karaagaoglu. easyROC: An Interactive Web-tool for ROC Curve Analysis Using R Language Environment. *The R Journal* **Vol. 8/2**, (2016).
35. Revelle, W. R. (Photographer). (2017). psych: Procedures for Personality and Psychological Research. Software.
36. Lê, S., Josse, J. & Husson, F. **FactoMineR**: An *R* Package for Multivariate Analysis. *J. Stat. Soft.* **25**, (2008).
37. R Core Team (2020). R: A language and environment for statistical computing. R Foundation for Statistical Computing, Vienna, Austria. URL https://www.R-project.org/.

Figures

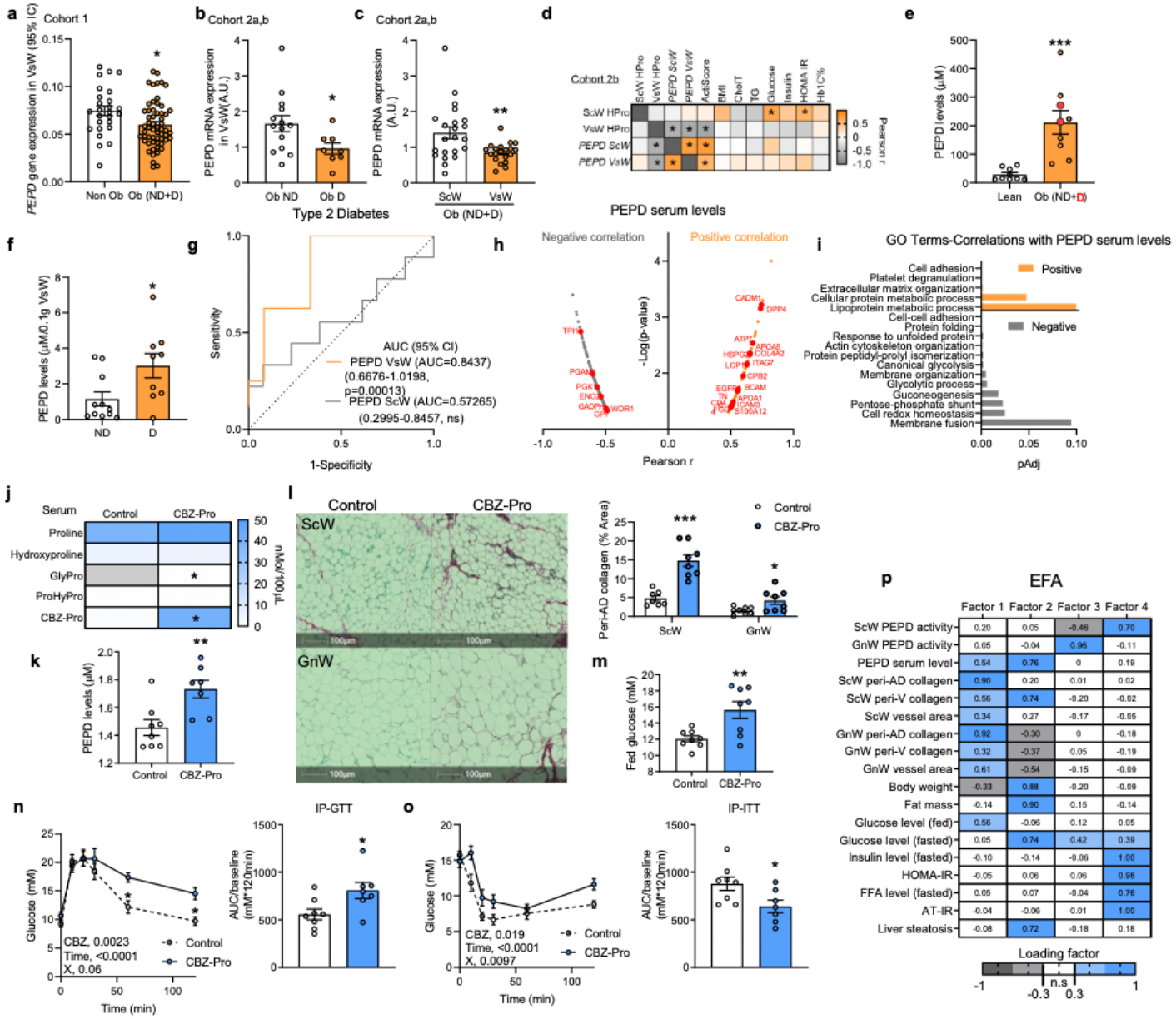

Figure 1

Obesity reduces AT PEPD activity and promotes PEPD release in association with AT fibrosis and insulin resistance. a-c, PEPD gene expression in VsW from non-obese (n=26) and obese (n=58) subjects from cohort 1 (a), in ScW and VsW (visceral, omental depot) obese non diabetic (Ob ND, 14) and diabetic (Ob D, n=8) subjects from cohort 2a, b (b, c). d, Pearson correlation matrix between ScW and VsW ECM remodelling markers and metabolic parameters in obese subjects from cohort 2b (n=14). e, ELISA analysis of PEPD levels in serum from lean (n=9) and obese non diabetic (ND) or diabetic (D, red dots) (n=9) subjects from cohort 2d, e. f, ELISA analysis of PEPD levels from VsW explants medium of obese diabetic (D, n=9) and non-diabetic (ND, n=12) subjects from cohort 2e, f. g, Area under the receiver operating curve (AUC) values (95% CI) for PEPD VsW levels from cohort 2e,f to discriminate subjects with

type 2 diabetes. h, i, PEPD-protein correlations for Hyungwon Choi etal. cohort11, shown as volcano plots and GO enrichment analysis of the corresponding proteins. j, k, m, Proline metabolism-related amino acids serum level (j), PEPD serum levels (k) and fed glucose levels (m) in CBZ-Pro-treated mice (n=8) and littermates controls (n=8). l, Representative images of red Sirius staining in ScW and GnW of control (n=8) and CBZ-Pro treated mice (n=8) and corresponding quantification of peri-adipocyte collagen deposition represented in % Area (peri-AD collagen). n, o, Blood glucose levels up to 120 minutes after an intraperitoneal injection of glucose (2g/kg) in a glucose tolerance test (n) or insulin (0.75 IU/kg) in an insulin tolerance test (o) with the representative AUC in control (n=8) and CBZ-Pro treated mice (n=8). p, Heat map representing the four factors extracted through exploratory factor analysis. The columns report the factors loadings of the observed variables. *p<0.05 compared to non-obese (a), Ob ND (b), ScW(c), lean (e) ND (f), control (j-o) using t-test. 2way ANOVA with Turkey's post-hoc multiple comparisons test; G, genotype; X, interaction (n, o).

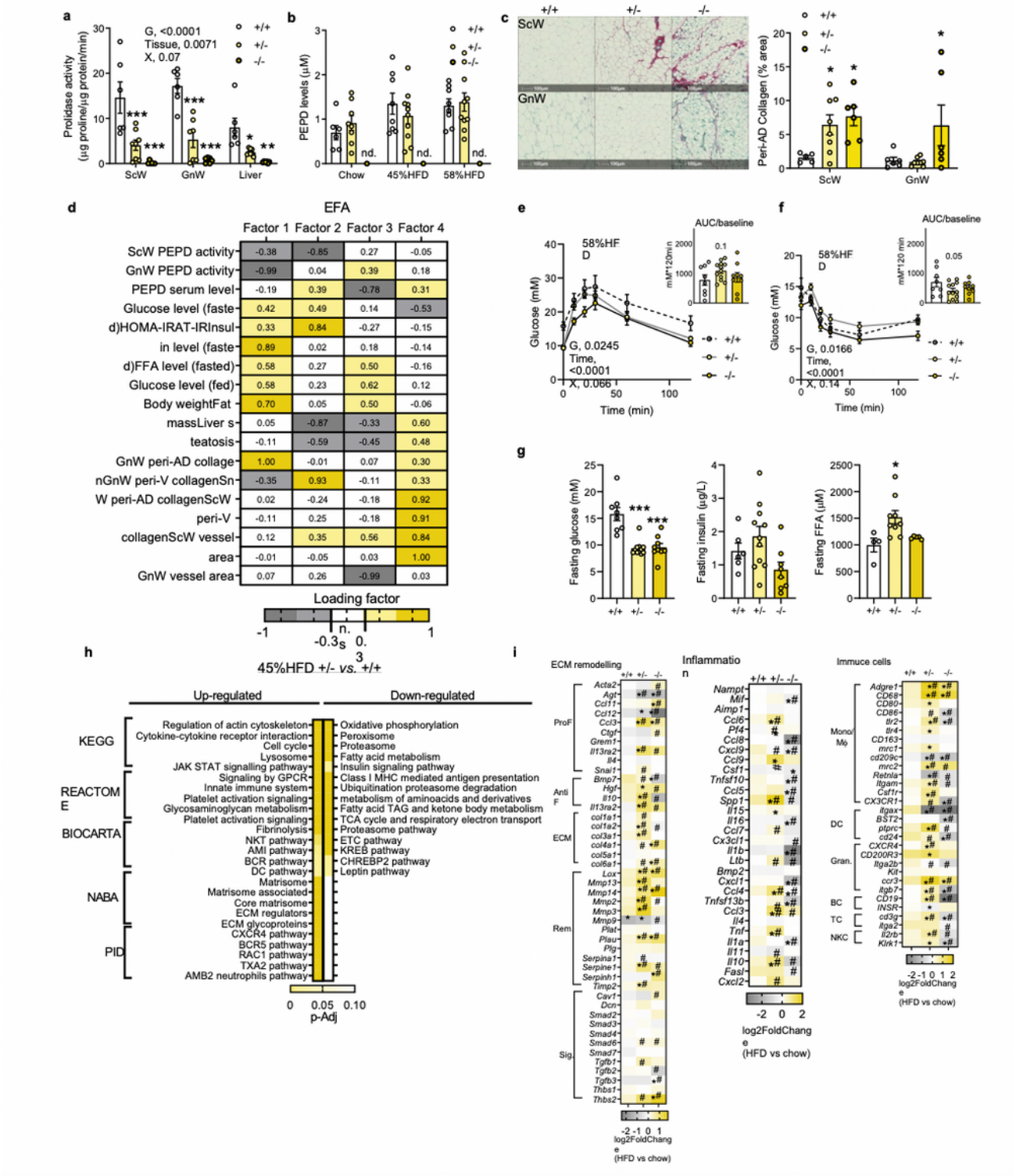

Figure 2

Pepd silencing exacerbates AT fibro-inflammation and metabolic dysfunctions in DIO mice. a. Prolidase activity in ScW, GnW and liver from pepd WT (n=6), HET (n=8) and KO mice (n=5); b. ELISA analysis of PEPD levels in the serum of pepd WT (6) and HET (10) fed chow. c. Representative images of red Sirius staining in ScW and GnW from pepd WT (n=6), HET (n=8) and KO (n=6) mice fed chow and quantification of peri-adipocyte collagen % area (peri-AD collagen). d. Heat map representing the four

factors extracted through exploratory factor analysis. The columns report the factors loadings of the observed variables. e, f. Blood glucose levels up to 120 min. after an intraperitoneal injection of glucose in a glucose tolerance test (e) or insulin (0.75 IU/kg) in an insulin tolerance test (f) with the representative AUC in pepd WT (n=8), HET (n-11) and KO (n=9) mice fed HFD 58%. g. Fasting glucose, insuli n and FFA levels in pepd WT (n=8), HET (n-11) and KO (n=9) mice fed HFD 58%. h. Pathway enrichment analysis of the DEGs in GnW from pepd HET (C, n=10) and KO (D, n=9) mice compared to WT mice (n=8) fed HFD 45%, using different data bases (KEGG, Reactome, Biocarta, NABA and PID). The heat maps indicate the level of significant changes (false discovery rate-adjusted p-value).i. Heat maps of fibro-inflammatory related DEGs in GnW of pepd WT, HET and KO mice in HFD 45% (8, 10, 9, respectively) expressed as Log2 fold change (Log2FC) variation over chow diet (n=4, 8, 5, respectively). ProF (pro-fibotic); AntiF (anti-fibrotic); Rem (ECM remodeling); Sig. (ECM-related signaling); Mono/Mφ (monocyte/macrophage); DC (dendritic cell); Gran. (granulocyte); BC (B cell); TC (T cell); NKC (natural killer cell). *p-Adj<0.1, significant DEG compared to chow diet. #q<0.05 compared to pepd WT (+/+).*p<0.05 compared to +/+ using One way ANOVA with Sidak's (e, f) or Dunnett's (c, g) post-hoc multiple comparisons test. 2way ANOVA with Turkey's post-hoc multiple comparisons test; G, genotype; X, interaction (a, b, e, f).

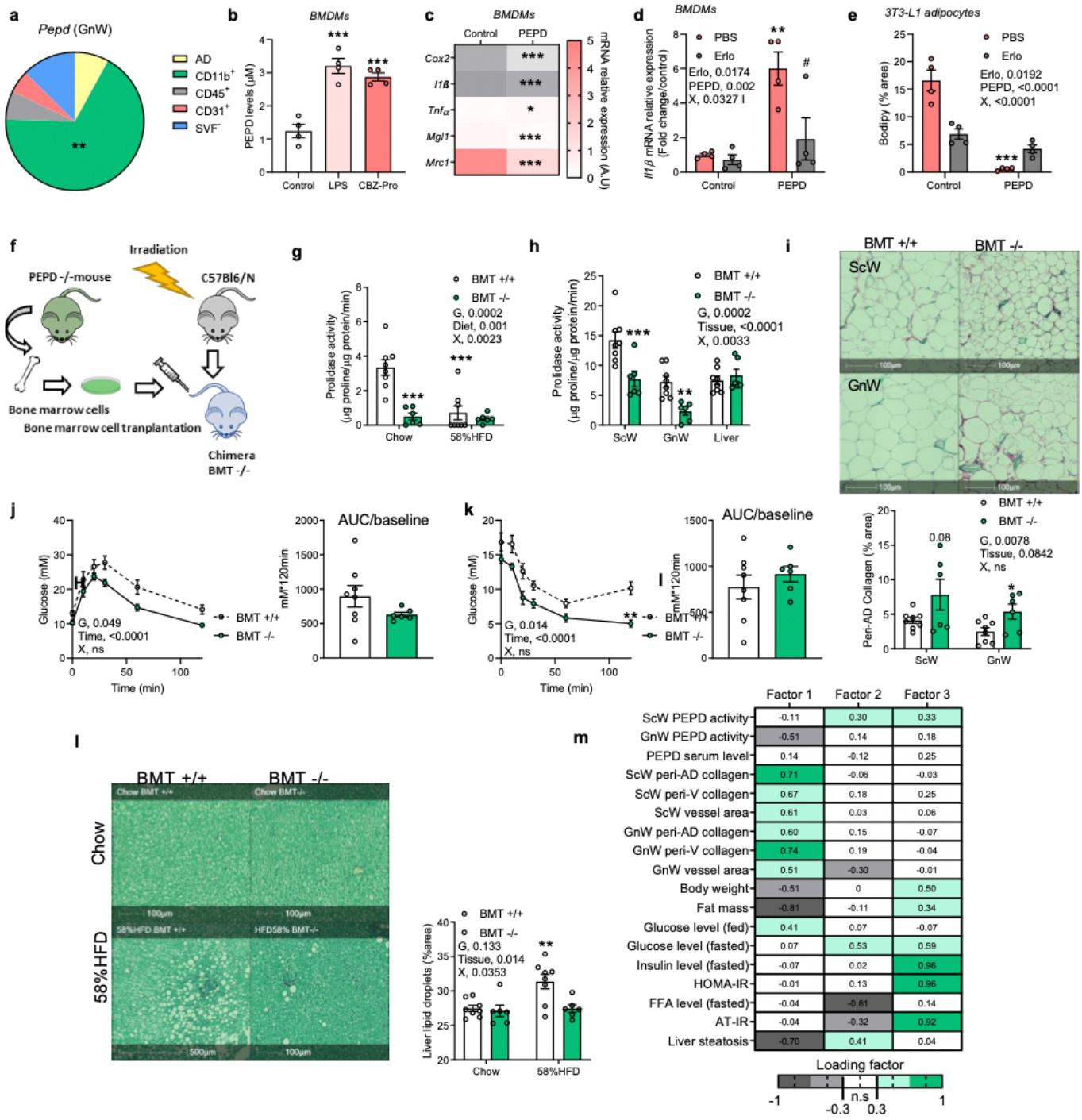

Figure 3

Hematopoietic-specific pepd silencing reduced AT fibro-inflammation and improves insulin sensitivity in obese mice. a. Pie chart illustration of Pepd mRNA relative expression distribution in GnW from C57Bl/6 mice fed chow diet (n=4). AD, adipocytes; CD11b+, M□; CD45+, immune cells; CD31+ endothelial cells and SVF-, negative stroma-vascular fraction. b. PEPD released level from BMDMs treated or not (control, n=12) 24h with LPS (n=6) or CBZ-Pro (n=8). c. Heat map of gene expression in BMDMs after 4h

treatment with purified PEPD protein (n=4). d, e. IL1β mRNA relative expression in BMDMs (n=4, d) or in 3T3-L1 adipocytes (n=4, e) pre-treated (Erlo) or not (PBS) with Erlotinib 5µM prior treatment with (PEPD) or without (control) purified PEPD protein (250nM) for 24h (d) or during the first 5 days of adipogenic differentiation (e). * compared to control PBS, # compared to PEPD PBS. f. Scheme of the bone marrow transplant strategy. g, h. Prolidase activity in peritoneal M (g), BAT, SCW, GnW and liver (h) from BMT WT (n=8) mice compared to BMT KO mice (n=6). i. Representative images of red Sirius staining ScW and GnW from BMT-WT (n=8) mice compared to BMTKO mice (n=6) fed chow and quantification of peri-AD collagen represented as %). j, k. Blood glucose levels up to 120 min. after an intraperitoneal injection of glucose (2g/kg) in a glucose tolerance test (j) or insulin (0.75 IU/kg) in an insulin tolerance test (k) in BMT WT (n=8) and KO mice (n=6) fed HFD 58% for 20 weeks. Respective AUC are represented. l. Representative images of red Sirius staining in Liver and quantification of liver steatosis expressed as % lipid droplets area. *compared to BMT +/+ chow. #p<0.05 compared to BMT +/+ HFD 58%. m. Heat map representing the four factors extracted through exploratory factor analysis. The columns report the factors loadings of the observed variables. *p<0.05, compared to control PEPD 0mM using a 1way ANOVA with Dunnett’s post-hoc multiple comparisons test (b). *p<0.05 compared to control using t-test (c, j, k). 2way ANOVA with Turkey’s multiple comparisons test (d, e, g-l); G, genotype; X, interaction.

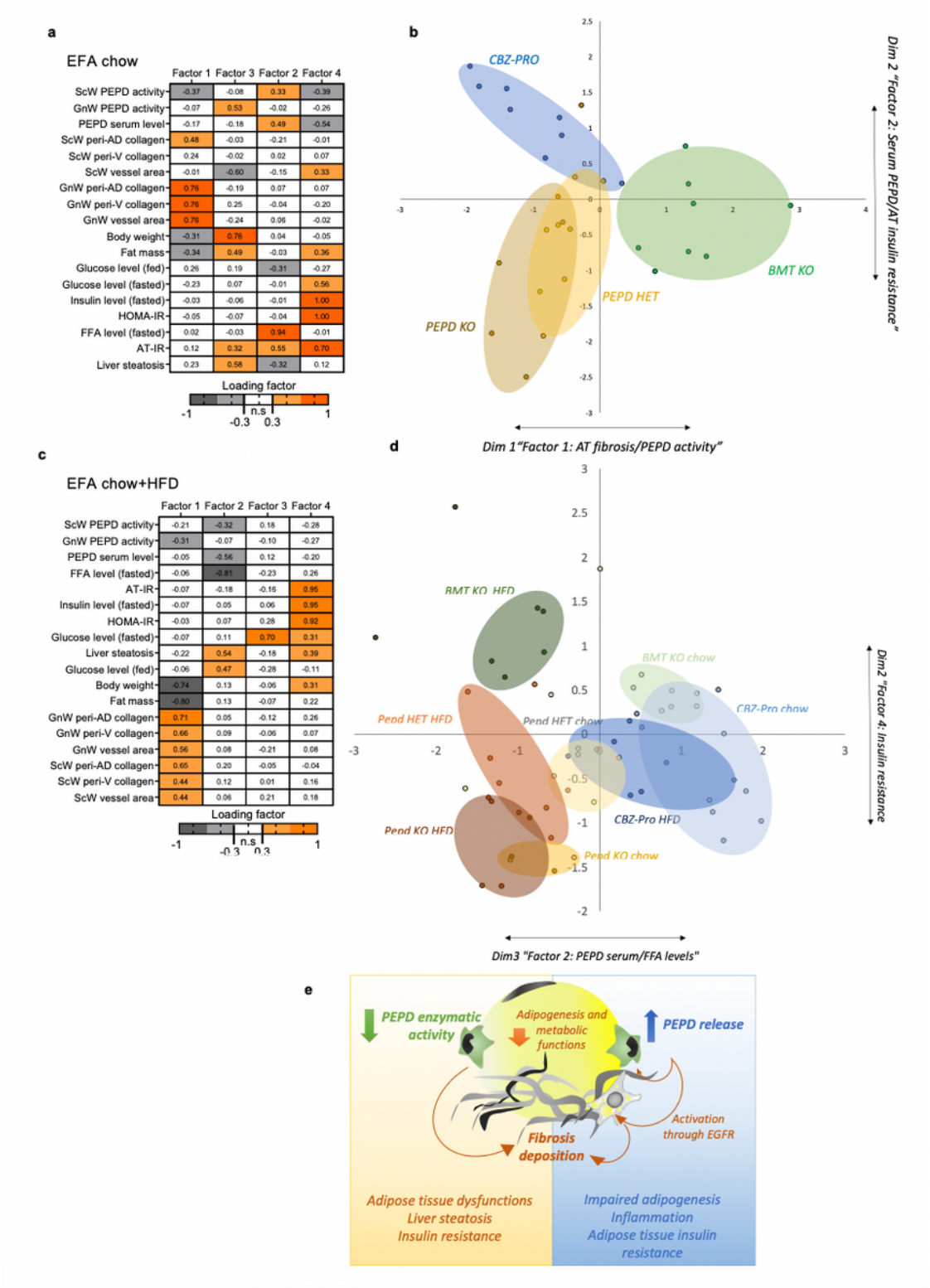

Figure 4

High PEPD serum levels is associated with AT insulin resistance and drives the differences between the pharmacologic and genetic animal models of PEPD down-regulation. a, b Heat map representing the four factors extracted through EFA performed among mice fed chow. The columns report the factors loadings of the observed variables. Mice from the three animal models (i.e. CBZ-Pro, PEPD and BMT) were plotted according to factor 1 and 2 (b). c, d. Heat map representing the four factors extracted through EFA

performed among mice fed chow+HFD. The columns report the factors loadings of the observed variables. Mice from the three animal models (i.e. CBZ-Pro, PEPD and BMT) were plotted according to factor 2 and 4 (d). Each colour corresponds to a group of animal. e. Summary of proposed roles of PEPD in obesity-associated AT dysfunctions and metabolic complications.

Supplementary Files

This is a list of supplementary files associated with this preprint. Click to download.

- PellergrinelliEtalNatSI.docx
- SupplementaryInformationSupplementaryTableS2.xlsx
- SupplementaryInformationSupplementaryTableS3.xlsx
- SupplementaryInformationSupplementaryTableS4.xlsx
- SupplementaryInformationSupplementaryTableS5.xlsx
- SupplementaryInformationSupplementaryTableS6.xlsx
- SupplementaryInformationSupplementaryTableS7.xlsx
- SupplementaryInformationSupplementaryTableS8.xlsx
- PellergrinelliEtalNatExtendedData.docx